J. Fluid Mech. (1992), *vol.* 239, *pp.* 23–45
Printed in Great Britain

Sand ripples under sea waves
Part 3. Brick-pattern ripple formation

By G. VITTORI AND P. BLONDEAUX
Hydraulic Institute, University of Genoa, Via Montallegro, 1, 16145 Genoa, Italy

(Received 2 January 1991 and in revised form 6 August 1991)

An oscillatory flow over a cohesionless bottom can produce regular three-dimensional bedforms known as brick-pattern ripples characterized by crests perpendicular to the direction of fluid oscillations joined by equally spaced bridges shifted by half a wavelength between adjacent sequences (a photo of brick-pattern ripples is shown in Sleath 1984, p. 141). In the present paper brick-pattern ripple formation is explained on the basis of a weakly nonlinear stability analysis of a flat cohesionless bottom subject to an oscillatory flow in which three-dimensional perturbations are considered. It is shown that brick-pattern ripples are generated by the simultaneous growth of two-dimensional and three-dimensional perturbations which interact with each other, according to a mechanism similar to that described by Craik (1971) in a different context, forming a resonant triad. A comparison between the present theoretical finding and experimental data by Sleath & Ellis (1978), concerning the region of existence of brick-pattern ripples in the parameter space and their geometrical characteristics, supports the validity of the present approach.

1. Introduction

Many recent experimental and theoretical works have been devoted to the study of the generation and development of bedforms underneath sea waves, because of the importance of this subject in connection with coastal sediment transport.

A predictive theory of ripple formation based on a linear stability analysis of a flat cohesionless bottom subject to an oscillatory flow has recently been proposed by Blondeaux (1990). In Blondeaux (1990) the conditions for damping or amplification of an infinitesimal two-dimensional bottom perturbation and the wavelength of its most unstable component are determined. In particular it is shown that for fixed values of the Reynolds number R_δ of the bottom boundary layer and of the Reynolds number R_d of the sediments, a critical value $(F_d)_c$ of the sediment Froude number F_d exists below which every bottom perturbation decays and above which bottom perturbations with wavenumbers falling within a restricted range amplify.

Here R_δ, R_d and F_d are defined using the amplitude U_0^* of the velocity oscillations close to the sea bed, the Stokes boundary-layer thickness $\delta^* (= (2\nu/\omega^*)^{\frac{1}{2}}$ where ω^* is the angular frequency of sea waves and ν kinematic viscosity of water), the mean sediment grain size d^*, the ratio s between sediment and water densities and the acceleration due to gravity g: $R_\delta = U_0^* \delta^*/\nu$; $R_d = U_0^* d^*/\nu$; $F_d = U_0^*/[(s-1) g d^*]^{\frac{1}{2}}$.

Blondeaux (1990) predicts the appearance of two-dimensional ripples and their initial wavelength. However his analysis neglects nonlinear effects and cannot follow the temporal development of a finite-amplitude perturbation; hence it cannot predict a possible equilibrium amplitude of two-dimensional perturbations and

discriminate between rolling-grain and vortex ripples. The characteristics of the different kinds of ripples are given in Allen (1984) and Sleath (1984).

Nonlinear terms are taken into account in Vittori & Blondeaux (1990) where a weakly nonlinear stability analysis has been developed. The actual height and wavelength of two-dimensional ripples are predicted in a neighbourhood of the critical conditions in the absence of flow separation. Assuming that the latter occurs at the ripple crest when the ratio K between ripple height and wavelength is larger than 0.1, the analysis developed in Vittori & Blondeaux (1990) also allows one to determine the conditions for incipient formation of vortex ripples.

All the studies performed so far assume the bed configuration and the flow field to be two-dimensional. As previously pointed out, experimental evidence exists that, under particular conditions, three-dimensional bedforms might appear.

While the present work was in progress, an attempt to explain the appearance of three-dimensional bottom configurations underneath sea waves and in particular of brick-pattern ripples was published (Hara & Mei 1990). They examine the stability of the oscillatory flow over a fixed two-dimensional wavy wall with respect to three-dimensional perturbations. They find that three-dimensional perturbations of the flow field, which are subharmonic in the longitudinal direction with respect to the bottom waviness, may grow depending on the values of the relevant physical parameters. Considering the mean shear stress that these flow perturbations induce on the bottom, Hara & Mei (1990) argue that brick-pattern ripples may be generated, the sediment being driven by bottom stresses associated with flow perturbations. Our view differs from theirs: we feel that the mechanism leading to the formation of brick-pattern ripples arises from an instability of sediment motion which occurs on space and time scales different from those characteristic of the flow instability mechanism described by Hara & Mei (1990). A comparison performed by Hara & Mei (1990) between their theoretical findings and the experimental data of Sleath & Ellis (1978) clearly shows that: (i) brick-pattern ripples were detected by Sleath & Ellis (1978) for values of the dimensionless parameter T (defined as $T = \sqrt{2}a^* U_0^{*2}(\delta^* l^{*2}\omega^{*2})^{-1}$, with a^* and l^* ripple amplitude and longitudinal wavelength respectively) well below the critical value T_c predicted by Hara & Mei (1990) for brick-pattern ripple formation. Indeed for the experimental conditions of Sleath & Ellis (1978) the value of T_c predicted by the analysis of Hara & Mei (1990) is found to be 2.06 while the experimental values of T range between 1.02 and 1.83; (ii) the experimental values of transverse wavelengths of brick-pattern ripples are much longer than the values computed on the basis of Hara & Mei's (1990) theory. In fact for the experimental conditions of Sleath & Ellis (1978), Hara & Mei (1990) predict a transverse wavelength approximately equal to $8.5\delta^*$, while the brick-pattern ripples observed by Sleath & Ellis (1978) are characterized by an average transverse wavelength approximately equal to $27.5\delta^*$. However, even though in the literature sea and river bedforms are invariably found to be produced typically by the instability of sediment motion with the secondary flow of the fluid passively driven by the bottom perturbations (Fredsøe 1974; Parker 1976; Richards 1980; Sumer & Bakioglu 1984; Blondeaux & Seminara 1985; Colombini, Seminara & Tubino 1987), values of the parameters may exist such that the length- and timescales characteristic of the flow instability mechanism described by Hara & Mei (1990) become comparable with those found by analysing the stability of the bottom and in this case the two mechanisms may interact.

In the present work it is shown that the formation of brick-pattern ripples can be explained on the basis of a weakly nonlinear stability analysis of a flat cohesionless

bottom subject to an oscillatory flow in which three-dimensional perturbations of the bottom profile are considered. In particular the present analysis shows that brick-pattern ripples are generated by the simultaneous growth of two-dimensional and three-dimensionl bottom perturbations which interact with each other with a mechanism similar to that described by Craik (1971) in a different context. Depending on the values of the parameters this nonlinear interaction leads to an energy transfer from the two-dimensional perturbations to the three-dimensional ones or vice versa and brick-pattern ripples may appear even when a linear stability analysis predicts the appearance of two-dimensional ripples or the growth of a purely three-dimensional bottom perturbation. A comparison between the present theoretical findings and experimental data by Sleath & Ellis (1978) supports the validity of the present approach.

The procedure used in the rest of the paper is the following: in the next section we investigate the time development of infinitesimal three-dimensional bottom perturbations of the sea bed under the action of surface gravity waves. In particular it is shown that three-dimensional bottom perturbations may be more unstable than two-dimensional ones. In §3 the interaction of two-dimensional and three-dimensional perturbations of small but finite amplitude is considered within a neighbourhood of the critical conditions. In particular the growth of three-dimensional and two-dimensional perturbations is investigated for values of the parameters of the perturbations such that they form a resonant triad (Craik 1971). It is shown that the simultaneous growth of two-dimensional and three-dimensional perturbations leads to a bottom configuration similar to that of brick-pattern ripples. Finally the relevance of the theory in explaining brick-pattern ripple formation is discussed.

2. Three-dimensional bottom perturbation: linear analysis

2.1. *Formulation of the problem*

We follow Blondeaux (1990) and consider a two-dimensional gravity wave of small height H^*, length L^* and period T^* in shallow water of depth D^* propagating over an initially flat cohesionless bottom formed by sediment of uniform size d^*, density ρ_s and porosity n. Let us denote by ρ and ν the density and kinematic viscosity of water respectively.

It is well established that the flow can be modelled as irrotational except within the unsteady layer adjacent to the bottom. Since we are interested in the interaction between fluid and sediment, we focus our attention on that boundary layer and use linear wave theory to describe the motion outside this region. We define a Cartesian orthogonal coordinate system (x^*, y^*, z^*) with the x^*-axis lying on the bottom and parallel to the direction of wave propagation and the y^*-axis directed upward. Under the assumptions described in Blondeaux (1990), i.e. that the characteristic thickness of the bottom boundary layer is much smaller than both the water depth and the length of the gravity wave, we can assume the following form of the velocity vector $\boldsymbol{v}^* = (u^*, v^*, w^*)$ outside the bottom layer

$$\boldsymbol{v}^* = (u^*, v^*, w^*) = (-\tfrac{1}{2}U_0^* \, \mathrm{e}^{\mathrm{i}\omega^* t^*} + \text{c.c.}, 0, 0) \tag{1}$$

where t^* is time, $\omega^* = 2\pi/T^*$ is angular frequency of the sea wave, U_0^* is the amplitude of the irrotational velocity oscillations evaluated at the bottom and c.c. denotes the complex conjugate of a complex number.

If the bottom is flat and d^* is much smaller than the characteristic thickness of the bottom boundary layer $\delta^*(=(2\nu/\omega^*)^{\frac{1}{2}})$, the fluid motion is described by the well-known Stokes' (1851) solution and the sediment moves to and fro.

Let us now consider a bottom perturbation of the form

$$y^* = \eta^*(x^*, z^*, t^*) = \epsilon^* C(t^*)\, \mathrm{e}^{\mathrm{i}(\alpha^* x^* + \gamma^* z^*)} + \text{c.c.} \tag{2}$$

with wavenumbers α^* and γ^* in the x^* and z^* directions respectively and 'small' (strictly infinitesimal) amplitude $\epsilon^*\, C(t^*)$.

The problem of flow and bottom development is posed by Navier–Stokes equations, flow and sediment continuity equations with appropriate boundary conditions, namely the boundary-layer flow must match the outer irrotational motion and no slip is reinforced at the bottom surface.

Let us define the following dimensionless variables:

$$\left.\begin{aligned} (x, y, z) = (x^*, y^*, z^*)/\delta^*, \quad t = t^*\omega^*, \quad \epsilon = \epsilon^*/\delta^*, \quad \eta = \eta^*/\delta^*, \\ (\alpha, \gamma) = (\alpha^*, \gamma^*)\,\delta^*, \quad \boldsymbol{v} = (u, v, w) = (u^*, v^*, w^*)/U_0^*, \\ p = p^*/\rho(U_0^*)^2, \quad \boldsymbol{q} = (q_x, q_z) = \boldsymbol{q}^*/[(\rho_s/\rho - 1)\, g d^{*3}]^{\frac{1}{2}}, \end{aligned}\right\} \tag{3}$$

where $\boldsymbol{q}^*$ is the sediment flow rate which has components in the x- and z-directions. The governing differential problem then reads

$$\frac{2}{R_\delta}\frac{\partial \boldsymbol{v}}{\partial t} + \boldsymbol{v}\cdot\nabla\boldsymbol{v} = -\nabla p + \frac{1}{R_\delta}\nabla^2 \boldsymbol{v}, \tag{4}$$

$$\nabla\cdot\boldsymbol{v} = 0, \tag{5}$$

$$\nabla\cdot\boldsymbol{q} = -\frac{2F_d}{R_d}(1-n)\frac{\partial \eta}{\partial t}, \tag{6}$$

$$\boldsymbol{v} = (u, v, w) = (0, 0, 0) \quad \text{at} \quad y = \eta(x, z, t), \tag{7a}$$

$$\boldsymbol{v} = (u, v, w) \to (-\tfrac{1}{2}\mathrm{e}^{\mathrm{i}t} + \text{c.c.}, 0, 0) \quad \text{for} \quad y \to \infty, \tag{7b}$$

where the parameters – flow Reynolds number R_δ, particle Reynolds number R_d, particle Froude number F_d and the ratio between sediment and fluid densities s – are defined

$$R_\delta = \frac{U_0^*\,\delta^*}{\nu}, \quad R_d = \frac{U_0^*\, d^*}{\nu}, \quad F_d = \frac{U_0^*}{[((\rho_s/\rho) - 1)\, g d^*]^{\frac{1}{2}}}, \quad s = \frac{\rho_s}{\rho}. \tag{8}$$

In order to close the above formulation, we need a relationship between the sediment flow rate $\boldsymbol{q}^*$ and flow properties. As discussed in Blondeaux (1990) this can be simply obtained by relating $\boldsymbol{q}^*$ to the agitating forces which act on sediment grains. Here it is necessary to extend the relationship, taking into account that the bottom configuration is three-dimensional. We pose

$$\boldsymbol{q} = a\left|\frac{2}{R_d}\boldsymbol{V} - \frac{\mu}{F_d^2}\nabla\eta\right|^{(b-1)}\left(\frac{2}{R_d}\boldsymbol{V} - \frac{\mu}{F_d^2}\nabla\eta\right), \tag{9}$$

where $\boldsymbol{V}$ is the velocity vector evaluated at a distance from the bed equal to $\frac{1}{2}d^*$. The constant μ in (9) was introduced by Fredsøe (1978) in a different context. The values of a and b can be estimated in the relevant range of the parameters (i.e. for $R_d < R_\delta$) by requiring that relationship (9) should match the empirical law proposed by Grass & Ayoub (1982) in the two-dimensional case for small values of the grain size. A more

exhaustive discussion of (9) is presented in Blondeaux (1990) and in Vittori & Blondeaux (1990). The authors feel that (9) can be confidently used to study bottom development since it contains the main physical ingredients controlling the process of transport. However we point out that (9) can only be assumed appropriate within a linear context, but its extension to the weakly nonlinear case would involve complications which do not seem justified at this stage given the uncertainty which is still present in the estimate of the coefficients a, b and μ.

2.2. *Solution*

Since it is assumed that ϵ be a quantity much smaller than one, the solution of the problem formulated above can be expanded in power series of ϵ in the form

$$(u, v, w) = (u_0(y,t), 0, 0) + \epsilon C(t)\,(u_1(y,t), v_1(y,t), w_1(y,t))\,\mathrm{e}^{\mathrm{i}(\alpha x+\gamma z)} + \text{c.c.} + O(\epsilon^2), \quad (10)$$

$$p = p_0(y,t) + \epsilon C(t)\,p_1(y,t)\,\mathrm{e}^{\mathrm{i}(\alpha x+\gamma z)} + \text{c.c.} + O(\epsilon^2), \quad (11)$$

$$\boldsymbol{q} = (q_0(t), 0) + \epsilon C(t)\,(q_{x1}(t),\, q_{z1}(t))\,\mathrm{e}^{\mathrm{i}(\alpha x+\gamma z)} + \text{c.c.} + O(\epsilon^2). \quad (12)$$

By substituting from (10) and (11) into (4)–(7) and equating like powers of ϵ, at $O(\epsilon^0)$ the Stokes problem is found and the solution for u_0 can be readily obtained.

The problem at $O(\epsilon)$ reads

$$\frac{2}{R_\delta}\frac{\partial u_1}{\partial t} + \mathrm{i}\alpha u_0 u_1 + \frac{\partial u_0}{\partial y} v_1 = -\mathrm{i}\alpha p_1 + \frac{1}{R_\delta}\left[\frac{\partial^2 u_1}{\partial y^2} - (\alpha^2+\gamma^2)\,u_1\right], \quad (13a)$$

$$\frac{2}{R_\delta}\frac{\partial v_1}{\partial t} + \mathrm{i}\alpha u_0 v_1 = -\frac{\partial p_1}{\partial y} + \frac{1}{R_\delta}\left[\frac{\partial^2 v_1}{\partial y^2} - (\alpha^2+\gamma^2)\,v_1\right], \quad (13b)$$

$$\frac{2}{R_\delta}\frac{\partial w_1}{\partial t} + \mathrm{i}\alpha u_0 w_1 = -\mathrm{i}\gamma p_1 + \frac{1}{R_\delta}\left[\frac{\partial^2 w_1}{\partial y^2} - (\alpha^2+\gamma^2)\,w_1\right], \quad (13c)$$

$$\mathrm{i}\alpha u_1 + \frac{\partial v_1}{\partial y} + \mathrm{i}\gamma w_1 = 0, \quad (14)$$

$$C(\mathrm{i}\alpha q_{x1} + \mathrm{i}\gamma q_{z1}) = -(1-n)\frac{2F_d}{R_d}\frac{\mathrm{d}C}{\mathrm{d}t}, \quad (15)$$

$$(u_1, v_1, w_1) = \left(-\frac{\partial u_0}{\partial y}, 0, 0\right) \quad \text{at} \quad y = 0, \quad (16)$$

$$(u_1, v_1, w_1) \to (0,0,0) \quad \text{for} \quad y \to \infty. \quad (17)$$

In deriving the equations for u_1, v_1 and w_1, the time derivative of $C(t)$ has been assumed to be much smaller than $C(t)$ itself; thus the study of the flow field has been decoupled from that of bottom time development. The latter assumption, supported by experimental evidence, is formally justified assuming the quantity $[aR_d^{1-b}/(1-n)\,2F_d]$ to be small and taking into account that the velocity V is proportional to $R_\delta/2R_d^z$ with R_d much smaller than R_δ.

Introducing a coordinate system which moves with the fluid far from the bottom and after some manipulations involving much tedious algebra, it is possible to decouple flow equations (13)–(14) and to obtain an equation for the vertical component of velocity, which is similar to that found by Blondeaux (1990) for the stream function. The same analytical procedure of solution, which is essentially an extension of Seminara & Hall's (1976) procedure developed in a different context, can then be used.

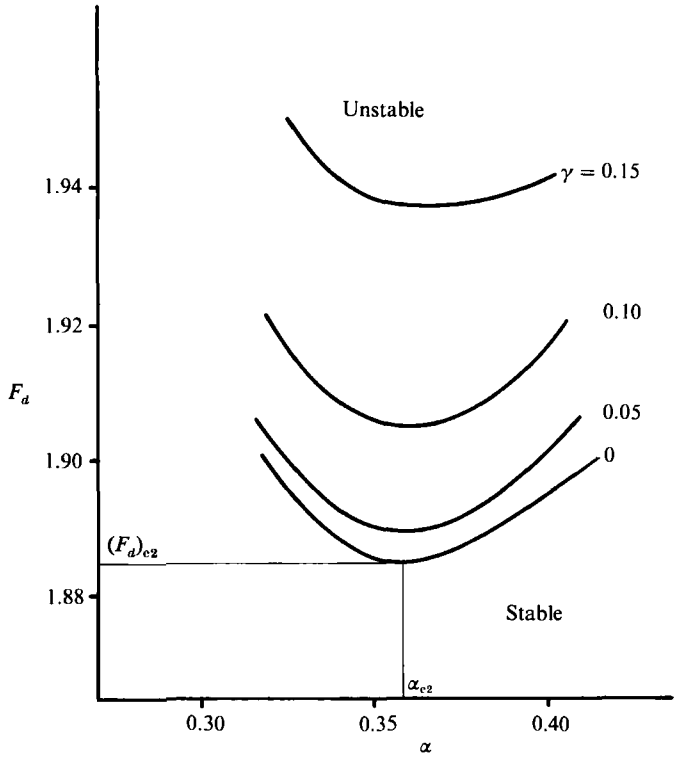

FIGURE 1. Marginal stability curves in an (α, F_d)-plane for different values of γ and $R_d = 20$, $R_\delta = 20$ ($s = 2.65$, $\mu = 0.15$).

Once v_1 is known, the analytical integration of (13b) gives the pressure field while w_1 can be determined by means of a procedure similar to that employed for v_1. Finally u_1 is provided by the continuity equation (14).

For brevity we skip the details, which are given in Vittori (1992) where results concerning the oscillatory flow over a three-dimensional bottom configuration are extensively discussed. Here we focus our attention on bottom time development.

Once the velocity field is known, one can easily solve for the bottom time development by substituting the transport rate formula into (15). It is easy to see that

$$\frac{\mathrm{d}C(t)}{\mathrm{d}t} = -\frac{aR_d^{1-b}}{2F_d(1-n)}|2u_0|^{b-1}\left\{2\left[\mathrm{i}\alpha b\left(u_1+\frac{\partial u_0}{\partial y}\right)+\mathrm{i}\gamma w_1\right] + \frac{\mu R_d}{F_d^2}[\alpha^2 b+\gamma^2]\right\}_{y=\frac{R_d}{2R_\delta}} C(t) = g(t)\,C(t), \quad (18)$$

whence

$$C(t) = C(0)\exp\left[\int_0^t g(\xi)\,\mathrm{d}\xi\right]. \quad (19)$$

As in the two-dimensional case, four contributions to $C(t)$ can be identified. The first two contributions are related to the real and imaginary parts of the time average of the function $g(t)$. The real part controls the amplification of the bottom perturbation, while the imaginary part gives the wave speed. The third and fourth contributions are related to the oscillatory part of g with a vanishing average. They

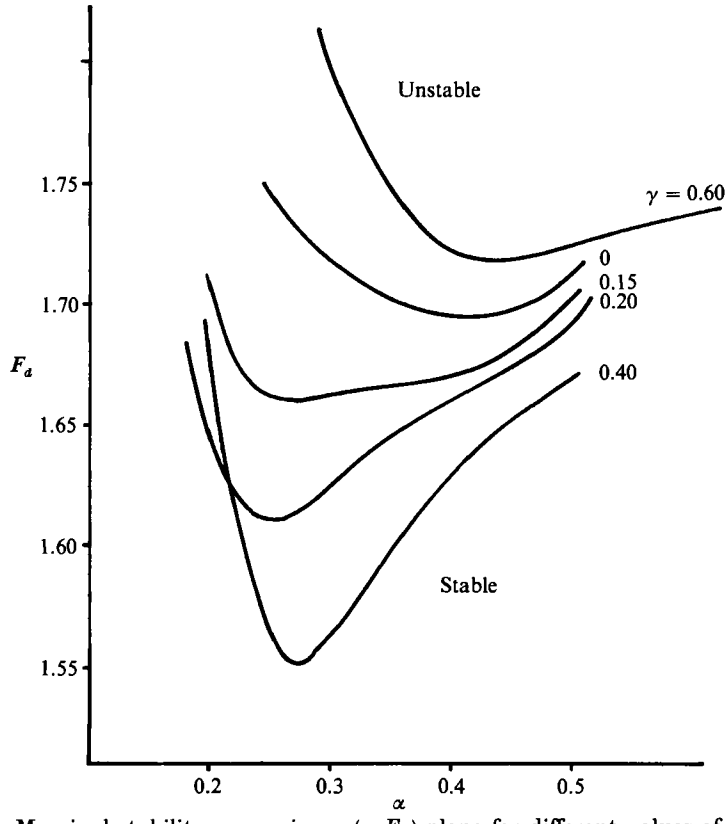

FIGURE 2. Marginal stability curves in an (α, F_d)-plane for different values of γ and $R_d = 10$, $R_\delta = 30$ ($s = 2.65$, $\mu = 0.15$).

describe the time variation of the perturbation profile around its average position during a wave cycle.

2.3. *Discussion of the results*

As previously pointed out, the growth or decay of three-dimensional bottom perturbations is related to the mean value of the real part of the function $g(t)$ appearing in (19), and, as discussed in Blondeaux (1990), two contributions to this mean value can be identified. The first is associated with the steady component of the fluid velocity evaluated at $y^* = \frac{1}{2}d^*$, the second is due to the component of gravity along the bed profile. While the latter has a stabilizing effect, the former may be stabilizing or destabilizing depending on the values of α, γ and R_δ, R_d.

For $\gamma = 0$ the behaviour of two-dimensional bottom perturbations is recovered. A detailed discussion of the results can be found in Blondeaux (1990). As already mentioned in the Introduction, for fixed values of R_δ and R_d there is a critical value $(F_d)_c$ of F_d below which every two-dimensional bottom perturbation decays and above which bottom perturbations with the longitudinal wavenumber α falling within a restricted range amplify. For non-vanishing values of γ, the same qualitative behaviour is found even though some quantitative differences appear. Figures 1 and 2 show the marginal stability curves drawn for different γ, for $R_\delta = 20$, $R_d = 20$ and for $R_\delta = 30$, $R_d = 10$ respectively. As shown in figure 2, values of R_δ and R_d are found such that some three-dimensional bottom perturbations are more unstable than two-dimensional ones.

The latter result seems in contradiction with experimental evidence. Indeed three-dimensional bed configurations described by (2) have never been observed, neither has a bottom topography given by

$$y^* = \epsilon^*[C_1(t)\,\mathrm{e}^{\mathrm{i}(\alpha^* x^* + \gamma^* z^*)} + C_2(t)\,\mathrm{e}^{\mathrm{i}(\alpha^* x^* - \gamma^* z^*)} + \text{c.c.}] \tag{20}$$

been detected. Incidentally we point out that for fixed α, bottom perturbations characterized by transverse wavenumbers γ and $-\gamma$ have the same amplification rate.

This discrepancy between the theoretical results of the linear stability analysis and experimental evidence can be explained by taking into account nonlinear effects. In the next section we show that, within a neighbourhood of the critical conditions and for values of the relevant parameters such that three-dimensional components of the bottom perturbation are the most unstable, resonant triads exist which also lead to the explosive growth of a two-dimensional component with a wavenumber twice that of the three-dimensional components and an amplitude of the same order of magnitude as that of the three-dimensional components. We show that this is the mechanism by which brick-pattern ripples appear.

Brick-pattern ripples may also appear when two-dimensional components are more unstable than three-dimensional components. In this situation an energy transfer from two-dimensional perturbations to the three-dimensional ones takes places which causes the explosive growth of three-dimensional components with a longitudinal wavelength twice that of two-dimensional components.

3. Nonlinear interaction of two-dimensional and three-dimensional bottom perturbations: brick-pattern ripple formation

3.1. *Formulation of the problem*

The above discussion suggests that nonlinear effects must be accounted for. Let us first consider values of the parameters (R_δ, R_d) for which two-dimensional perturbations are the most unstable ones and let us assume that the actual value of F_d differs by a small amount from the critical value $(F_d)_{c2}$ characteristic of two-dimensional perturbations. Let us investigate whether in a neighbourhood of the critical conditions, nonlinear effects may lead to an energy transfer to three-dimensional components of bottom perturbations. The case in which three-dimensional perturbations are more unstable than two-dimensional ones will be considered in the following.

As shown by Craik (1971), the interaction between two- and three-dimensional perturbations is particularly strong when three perturbations are considered: one two-dimensional and two three-dimensional. The longitudinal wavenumber of the three-dimensional components should be half of the two-dimensional component and the three-dimensional components should have opposite wavenumbers in the transverse direction.

The above ideas suggest considering the following structure of a bottom perturbation:

$$\begin{aligned} y = {} & \epsilon[A_1(\tau)\,C_1(t)\,\mathrm{e}^{\mathrm{i}\beta x} + A_2(\tau)\,C_2(t)\,\mathrm{e}^{\mathrm{i}(\alpha x + \gamma z)} + A_3(\tau)\,C_3(t)\,\mathrm{e}^{\mathrm{i}(\alpha x - \gamma z)} + \text{c.c.}] \\ & + \epsilon^2[B_1(\tau)\,D_1(t)\,\mathrm{e}^{\mathrm{i}\beta x} + B_2(\tau)\,D_2(t)\,\mathrm{e}^{\mathrm{i}(\alpha x + \gamma z)} + B_3(\tau)\,D_3(t)\,\mathrm{e}^{\mathrm{i}(\alpha x - \gamma z)} + \text{c.c.} \\ & + \text{terms proportional to } \mathrm{e}^{\mathrm{i}2\beta x},\ \mathrm{e}^{\mathrm{i}(2\alpha x + 2\gamma z)}, \ldots] + O(\epsilon^3), \end{aligned} \tag{21}$$

where ϵ is a small parameter defined as

$$F_d = (F_d)_{c2} + k_2\,\epsilon, \quad F_d = (F_d)_{m3} + k_3\,\epsilon. \tag{22}$$

Moreover let $\beta = \alpha_{c2}$ and $\alpha = \frac{1}{2}\beta$, i.e. $\alpha = \frac{1}{2}\alpha_{c2}$.

In (22) $(F_d)_{m3}$ is the marginal value of the Froude number corresponding to $\alpha = \frac{1}{2}\alpha_{c2}$ and to the given value of γ, α_{c2} being the critical wavenumber of the most unstable two-dimensional bottom perturbation. The results of the linear stability analysis show that for γ of order one $(F_d)_{m3}$ is close to $(F_d)_{c2}$ whence assumption (22) is reasonable. The time variable τ defined as

$$\tau = \epsilon t \tag{23}$$

describes the 'slow' growth (or decay) of bottom perturbations averaged over a wave cycle for conditions close to the marginal ones, while the amplitude functions C_i, D_i $(i = 1, 2, 3)$ describe the time development of perturbations during a wave cycle.

The velocity field up to order ϵ^2 is then expanded in the form

$$\begin{aligned}(u, v, w) = {} & (u_0(y,t), 0, 0) \\ & + \epsilon\{A_1(\tau)\,C_1(t)\,(u_{11}(y,t), v_{11}(y,t), 0)\,e^{i\beta x} \\ & \quad + A_2(\tau)\,C_2(t)\,(u_{12}(y,t), v_{12}(y,t), w_{12}(y,t))\,e^{i(\alpha x+\gamma z)} \\ & \quad + A_3(\tau)\,C_3(t)\,(u_{13}(y,t), v_{13}(y,t), w_{13}(y,t))\,e^{i(\alpha x-\gamma z)} + \text{c.c.}\} \\ & + \epsilon^2\{B_1(\tau)\,D_1(t)\,(u_{21}(y,t), v_{21}(y,t), 0)\,e^{i\beta x} \\ & \quad + B_2(\tau)\,D_2(t)\,(u_{22}(y,t), v_{22}(y,t), w_{22}(y,t))\,e^{i(\alpha x+\gamma z)} \\ & \quad + B_3(\tau)\,D_3(t)\,(u_{23}(y,t), v_{23}(y,t), w_{23}(y,t))\,e^{i(\alpha x-\gamma z)} + \text{c.c.} \\ & \quad + \text{terms proportional to } e^{i2\beta x}, e^{i(2\alpha x+2\gamma z)}, \ldots\}. \end{aligned} \tag{24}$$

Similar relationships hold for pressure p and sediment flow rate $\boldsymbol{q}$.

Substituting (24) into (4)–(7) and equating like powers of ϵ, at order ϵ^0 the Stokes problem is obtained. At order ϵ the solution can be found by following the procedure described in the previous section. Because of the assumptions (22), bottom perturbations neither amplify nor decay at this order, hence the functions $C_i(t)$ $(i = 1, 2, 3)$ are given by the sum of a constant which, without loss of generality, can be assumed equal to one, and periodic functions of order $aR_d^{(1-b)}/[2F_d(1-n)]$ with a vanishing time average. Moreover the functions $A_i(\tau)$ $(i = 1, 2, 3)$ are left unknown at this order of approximation and will be determined at higher order.

At order ϵ^2, equating terms of the equations proportional to $e^{i\beta x}$, $e^{i(\alpha x+\gamma z)}$, $e^{i(\alpha x-\gamma z)}$, we obtain three problems for the following sets of unknowns: $(u_{21}, v_{21}, w_{21}, p_{21}, q_{21x}, q_{21z})$, $(u_{22}, v_{22}, w_{22}, p_{22}, q_{22x}, q_{22z})$, $(u_{23}, v_{23}, w_{23}, p_{23}, q_{23x}, q_{23z})$ respectively.

We omit details of the problems at this order and of their solutions, since very long expressions are involved and knowledge of the flow field at this order is not needed to determine the function $A_i(\tau)$ $(i = 1, 2, 3)$, i.e. the average growth or decay of bottom perturbations. We only point out that the flow and pressure fields $u_{2i}, v_{2i}, w_{2i}, p_{2i}$ can be split up into two parts $(u'_{2i}, v'_{2i}, w'_{2i}, p'_{2i})$ and $(u''_{2i}, v''_{2i}, w''_{2i}, p''_{2i})$; the former satisfies a problem identical with that obtained for $u_{1i}, v_{1i}, w_{1i}, p_{1i}$ and then it can be stated $(u'_{2i}, v'_{2i}, w'_{2i}, p'_{2i}) \equiv (u_{1i}, v_{1i}, w_{1i}, p_{1i})$, while the latter satisfies a non-homogenous problem.

Let us focus our attention instead on the sediment continuity equation, which along with the sediment transport rate formula, leads to the following relationships:

$$B_1\frac{\mathrm{d}D_1}{\mathrm{d}t}=-\frac{aR_d^{1-b}}{(1-n)\,2(F_d)_{c2}}\left\{B_1D_1Q_1+\frac{\mathrm{d}A_1}{\mathrm{d}\tau'}C_1-A_1C_1a_1-A_2C_2A_3C_3b_1\right\}, \quad (25a)$$

$$B_2\frac{\mathrm{d}D_2}{\mathrm{d}t}=-\frac{aR_d^{1-b}}{(1-n)\,2(F_d)_{m3}}\left\{B_2D_2Q_2+\frac{\mathrm{d}A_2}{\mathrm{d}\tau'}C_2-A_2C_2a_2-A_1\bar{A}_3C_1\bar{C}_3b_2\right\}, \quad (25b)$$

$$B_3\frac{\mathrm{d}D_3}{\mathrm{d}t}=-\frac{aR_d^{1-b}}{(1-n)\,2(F_d)_{m3}}\left\{B_3D_3Q_3+\frac{\mathrm{d}A_3}{\mathrm{d}\tau'}C_3-A_3C_3a_3-A_1\bar{A}_2C_1\bar{C}_2b_3\right\}, \quad (25c)$$

where an overbar denotes the complex conjugate of a complex number and the expressions for a_i, b_i and Q_i $(i=1,2,3)$, are given in the appendix. In (25) for convenience the variable τ' has been introduced:

$$\tau'=\frac{aR_d^{1-b}}{(1-n)\,2F_d}\tau. \quad (26)$$

Note that: (i) the bottom profile at $O(\epsilon^2)$ exhibits the same spatial structure as the profile derived at order ϵ; (ii) because of the assumption (22) the average over a cycle of the quantities Q_i $(i=1,2,3)$ vanishes (see (18)); (iii) the values of u''_{2i} and w''_{2i} at $y=R_d/2R_\delta$ differ from the values of u''_{2i} and w''_{2i} at the bottom by a small amount, since underneath gravity waves the size of sediment grains is usually much smaller than the boundary-layer thickness. The unknown values of u''_{2i} and w''_{2i} at $y=R_d/2R_\delta$ are then assumed to coincide with u''_{2i} and w''_{2i} evaluated at $y=0$, neglecting terms of $O(R_d/2R_\delta)$; (iv) the values of u''_{2i} and w''_{2i} at $y=0$ can be expressed in terms of u_{1i} and w_{1i} by employing the bottom boundary conditions; (v) because of (iii)–(iv) the unknowns $(u''_{2i}, v''_{2i}, w''_{2i})$ do not appear in the coefficients of (25); (vi) from (18), (25) and (22), it appears that the functions C_i and D_i $(i=1,2,3)$, which describe the time variation of the perturbation profile during a wave cycle, are given by the sum of two terms: a constant, which can be assumed without loss of generality equal to one because of the presence of the functions A_i, B_i $(i=1,2,3)$, and a periodic function of t of order $[aR_d^{1-b}/(1-n)\,2F_d]$.

We then perform the average over a cycle of (25) and neglect terms of order $(aR_d^{1-b}/[(1-n)\,2F_d])$ (it is worth remembering that on the basis of experimental evidence the quantity $aR_d^{1-b}/[(1-n)\,2F_d]$ has been assumed to be smaller than 1 in §2.2 in order to decouple fluid flow from bottom time development). We finally obtain the following system of three ordinary differential equations for the amplitude functions $A_i(\tau)$ $(i=1,2,3)$:

$$\frac{\mathrm{d}A_1}{\mathrm{d}\tau'}=\langle a_1\rangle A_1+\langle b_1\rangle A_2A_3, \quad (27a)$$

$$\frac{\mathrm{d}A_2}{\mathrm{d}\tau'}=\langle a_2\rangle A_2+\langle b_2\rangle A_1\bar{A}_3, \quad (27b)$$

$$\frac{\mathrm{d}A_3}{\mathrm{d}\tau'}=\langle a_3\rangle A_3+\langle b_3\rangle A_1\bar{A}_2, \quad (27c)$$

where $\langle a_i\rangle$, $\langle b_i\rangle$ $(i=1,2,3)$ represent the time average of a_i, b_i $(i=1,2,3)$. It appears

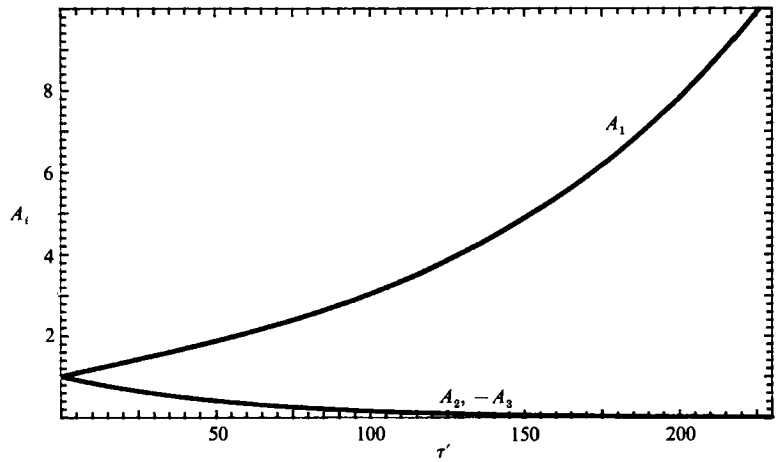

FIGURE 3. Time development of the amplitudes A_i $(i = 1, 2, 3)$ for $R_d = 30$, $R_\delta = 50$, $F_d = 2.15$, $\gamma = 0.14$, $\epsilon = 0.1$ ($s = 2.65$, $\mu = 0.15$). The initial value of the amplitudes is 1.0.

that the values of $\langle a_i \rangle$, $\langle b_i \rangle$ $(i = 1, 2, 3)$ depend on the parameters R_δ, R_d, F_d, s and can be evaluated without solving for the velocity field at order ϵ^2 (consider points iii and iv above).

3.2. *Discussion of the results*

The functions A_i $(i = 1, 2, 3)$ exhibit a variety of behaviour depending on their initial values and on the values of the coefficients appearing in (27). However a solution of the system (27) in closed form is not known. Some analytical solutions are presented for particular values of $\langle a_i \rangle$, $\langle b_i \rangle$ $(i = 1, 2, 3)$ by Weiland & Wilhelmsson (1977), Craik (1985), and others by Smith & Stewart (1987). In the present context the coefficients $\langle a_i \rangle$, $\langle b_i \rangle$ $(i = 1, 2, 3)$ are real. Moreover in order to study the formation of brick-pattern ripples, the functions A_i $(i = 1, 2, 3)$ will be assumed to be real, thus avoiding the analysis of the solution of the system (27) in the complex plane. Finally it can be checked that because of the symmetry of the problem $u_{12} \equiv u_{13}$ and $w_{12} = -w_{13}$. It follows

$$\langle a_2 \rangle = \langle a_3 \rangle, \quad \langle b_2 \rangle = \langle b_3 \rangle. \tag{28}$$

Moreover it can be assumed that

$$A_2 = -A_3. \tag{29}$$

The system (27) has been solved numerically using the Runge–Kutta method of fourth order.

At this stage it is useful to recall that, for given values of R_δ and R_d, the values of α, β, $(F_d)_{c2}$ are fixed. As a consequence $\langle b_1 \rangle$ and $\langle b_2 \rangle$ vary only with γ, but not with the actual value of F_d. On the other hand $\langle a_1 \rangle$ and $\langle a_2 \rangle$ are proportional to $F_d - (F_d)_{c2}$ and $F_d - (F_d)_{m3}$ respectively.

For given R_δ, R_d, F_d and γ two typical types of behaviour can be recognized, among others.

First (see figure 3) only A_1, i.e. the two-dimensional bottom perturbation, tends to amplify and thus the theory predicts the appearance of two-dimensional ripples. As explained in Vittori & Blondeaux (1990) rolling-grain ripples or vortex ripples will appear depending on the values of the relevant parameters.

Secondly (see figure 4) A_2 and A_3, i.e. the three-dimensional components of the bed

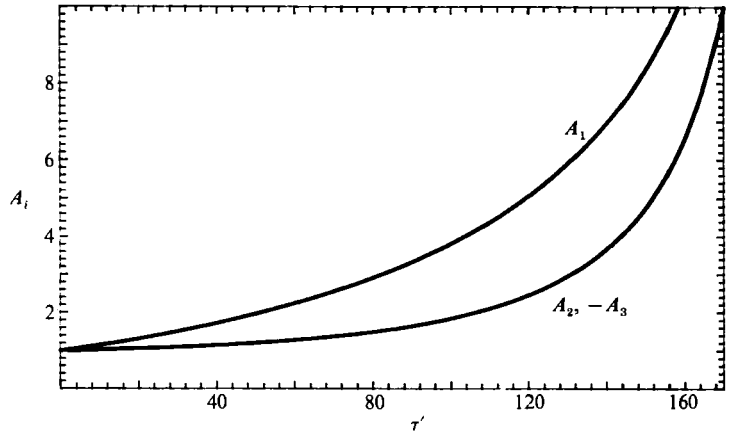

FIGURE 4. Time development of the amplitudes A_i ($i = 1, 2, 3$) for $R_d = 30$, $R_\delta = 68$. $F_d = 2.25$, $\gamma = 0.14$, $\epsilon = 0.1$ ($s = 2.65$, $\mu = 0.15$). The initial value of the amplitudes is 1.0.

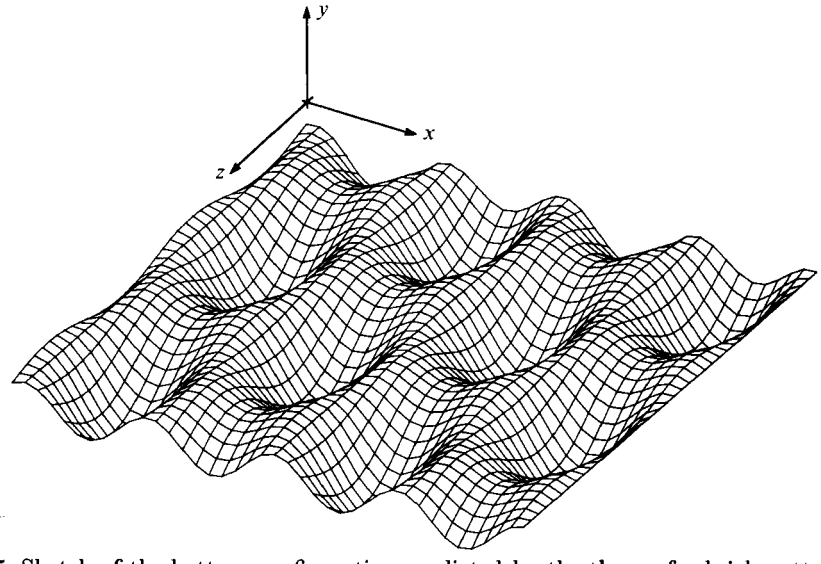

FIGURE 5. Sketch of the bottom configuration predicted by the theory for brick-pattern ripples.

perturbation, grow too giving rise to a bed configuration which is shown in figure 5 and is characteristic of brick-pattern ripples. Incidentally it is worth pointing out that the behaviour of A_i ($i = 1, 2, 3$) shown in figures 3 and 4 is respectively computed for values of the parameters close to those of experiments number 76 and 49 in table 1 of Sleath & Ellis (1978). As predicted by the present theory, in the former case Sleath & Ellis (1978) observed two-dimensional vortex ripples, while in the latter case the above authors detected brick-pattern ripples. Another example of the time development of the amplitude functions A_i is shown in figure 6. In this case the values of the parameters are close to those of experiment number 250 in table 1 of Sleath & Ellis (1978). Even though the values R_d and R_δ are smaller than those characteristic of experiment number 49, the behaviour of A_i is similar to that shown in figure 4. However the growth of the three-dimensional components is driven by the growth of the two-dimensional one when it assumes values larger than those

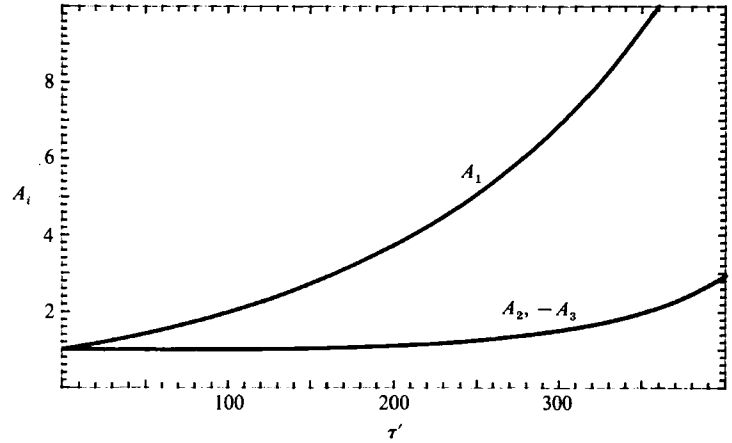

FIGURE 6. Time development of the amplitudes A_i $(i = 1, 2, 3)$ for $R_d = 20$, $R_\delta = 55$, $F_d = 2.05$. $\gamma = 0.1$, $\epsilon = 0.1$ ($s = 2.65$, $\mu = 0.15$). The initial value of the amplitudes is 1.0.

shown in figure 4. In both cases, the present results predict the appearance of brick-pattern ripples even though the Froude number is smaller than $(F_d)_{m3}$, i.e. for values of F_d such that a linear stability analysis would predict the damping of the three-dimensional components. Of course the appearance of brick-pattern ripples is also predicted for values of F_d larger than $(F_d)_{m3}$.

As previously pointed out, an analytical solution of the system (27) is known only for particular cases, hence we cannot provide a general criterion to predict the appearance of brick-pattern ripples, i.e. we cannot determine the range of values of R_δ, R_d and F_d for which brick-pattern ripples are expected to appear. Even experiments based on the numerical integration of (27) do not allow precise quantitative conclusions to be reached, since for fixed values of R_δ, R_d, F_d and γ the solution depends on the initial amplitudes of the various components of the bed perturbation. For example figure 7 shows the function A_i for the same values of the parameters as in figure 4 but different initial values of A_i, hereinafter referred to as A_{i0}. In particular from figure 7 (*a*) it can be appreciated that for $A_{i0} = 0.5$, the explosion of all the amplitudes A_i takes place almost at the same time for each component and $|A_2|$, $|A_3|$ reach an amplitude equal to 0.5 $|A_1|$ when the two-dimensional component has an amplitude of about 10. For $A_{i0} = 0.1$ (see figure 7*b*), the explosive growth of the amplitudes of the perturbation is delayed. At the initial stage, after a short time interval, the three-dimensional components are much smaller than the two-dimensional one and $|A_2|$, $|A_3|$ reach an amplitude of 0.5 $|A_1|$ only when the latter is approximately equal to 20. Finally, for $A_{i0} = 0.02$ (see figure 7*c*) the explosive growth of the two- and three-dimensional components is subject to a further delay and $|A_2|$, $|A_3|$ are equal to 0.5 $|A_1|$ only when the latter is extremely large. Since for the present approach to be rational the quantities ϵA_i $(i = 1, 2, 3)$ should be much smaller than 1, it follows that the appearance of brick-pattern ripples is rigorously predicted in a neighbourhood of the critical conditions, the size of which decreases as smaller values of A_{i0} are considered.

Let us assume that the initial amplitude of perturbations be not large, thus avoiding the possibility of a subcritical instability, i.e. the growth of pertubations in the region where a flat bed is stable as predicted by a linear stability analysis. The latter phenomenon may occur when the amplitudes A_i $(i = 1, 2, 3)$ are so large that nonlinear terms provide the necessary supply of energy to the perturbations.

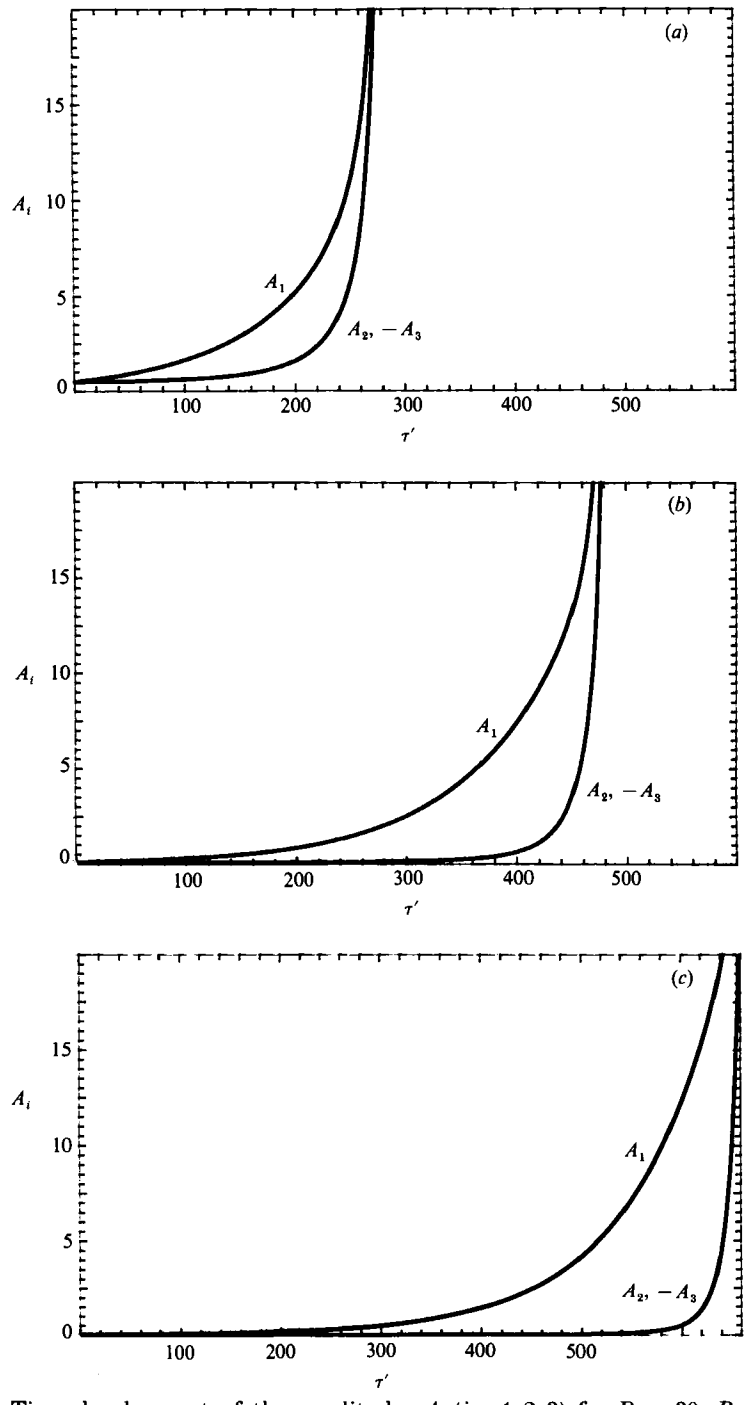

FIGURE 7. Time development of the amplitudes A_i ($i = 1, 2, 3$) for $R_d = 30$, $R_\delta = 68$, $F_d = 2.25$, $\gamma = 0.14$, $\epsilon = 0.1$ ($s = 2.65$, $\mu = 0.15$). The initial value of the amplitudes is (*a*) 0.5, (*b*) 0.1, (*c*) 0.02.

Let us start by considering the case $R_d = 40$ and R_δ falling within the range (0,100) which are values of the dimensionless parameters of physical relevance; here two-dimensional perturbations are always found to be more unstable than three-dimensional ones.

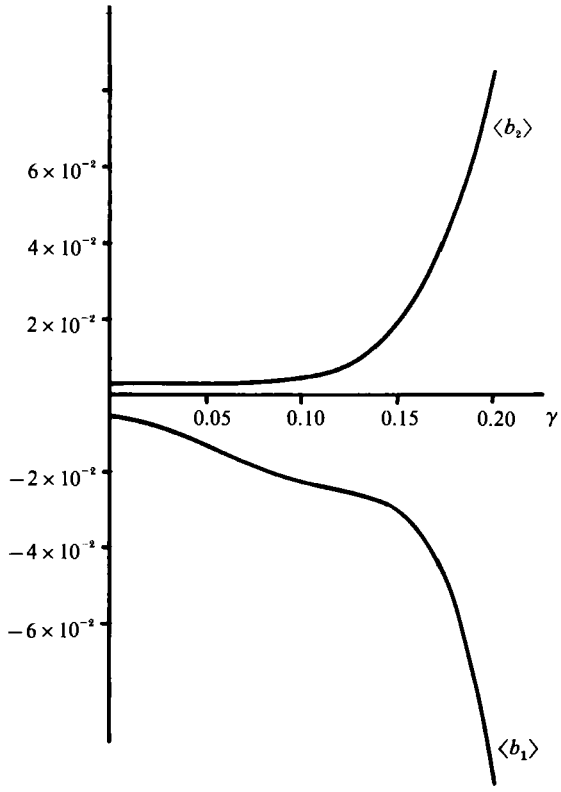

FIGURE 8. The coefficients $\langle b_1 \rangle$ and $\langle b_2 \rangle$ plotted versus γ for $R_d = 40$, $R_\delta = 60$, $\beta = 2\alpha = 0.253$ ($s = 2.65$, $\mu = 0.15$).

Look at the behaviour of bottom perturbations for values of the parameters falling in a neighbourhood of the critical conditions, i.e. considering values of F_d close to $(F_d)_{c2}$ and $(F_d)_{m3}$, numerical experiments seem to indicate that the simultaneous growth of the two-dimensional and three-dimensional perturbations is present when $\langle b_1 \rangle$ and $\langle b_2 \rangle$ are both negative and either $\langle a_1 \rangle$ or $\langle a_2 \rangle$ is positive.

Thus for given R_δ two alternatives arise which are discussed below.

(i) In the first case $\langle b_1 \rangle$ and $\langle b_2 \rangle$ are never simultaneously negative whatever value of γ is considered (see figure 8). In this situation brick-pattern ripples do not appear. If F_d is smaller than $(F_d)_{m3}$, (negative values of k_3) this result appears obvious since three-dimensional perturbations are then linearly stable. On the other hand it may be surprising that three-dimensional perturbations do not grow when F_d exceeds $(F_d)_{m3}$ (positive values of k_3). The decay of the three-dimensional components of the bottom perturbation is due to nonlinear terms which cause an energy transfer from the three-dimensional components to the two-dimensional one.

(ii) In the second case there is a range of γ within which $\langle b_1 \rangle$ and $\langle b_2 \rangle$ are both negative (see figure 9). When F_d is larger than $(F_d)_{c2}$ but smaller than $(F_d)_{m3}$ (k_2 positive and k_3 negative), a linear stability theory would predict the appearance of two-dimensional ripples. However, on the basis of the present work we can state that brick-pattern ripples will appear. The nonlinear terms now transfer energy from the two-dimensional component of the bottom perturbation to the three-dimensional ones. In this case the theory also gives the longitudinal and transverse wavenumbers of brick-pattern ripples. Indeed for fixed values of R_δ and R_d, one can look for the

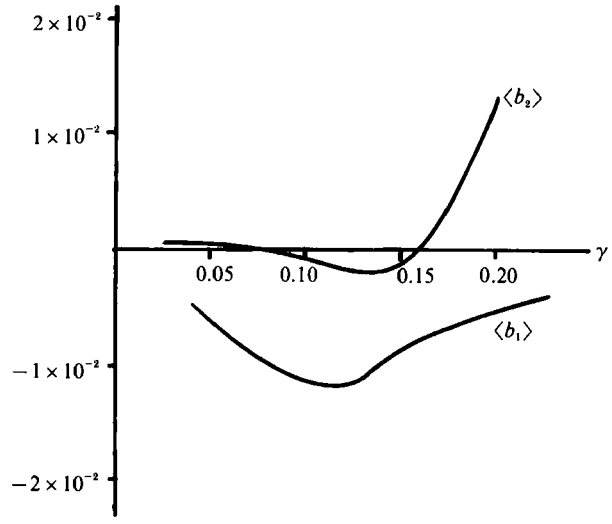

FIGURE 9. The coefficients $\langle b_1\rangle$ and $\langle b_2\rangle$ plotted versus γ for $R_d = 40$, $R_\delta = 80$, $\beta = 2\alpha = 0.250$ ($s = 2.65$, $\mu = 0.15$).

value of γ which causes the fastest growth of three-dimensional components of the bed perturbation. The longitudinal wavenumber is fixed by the condition $\alpha = \frac{1}{2}\alpha_{c2}$. Brick-pattern ripples also appear when F_d is larger than $(F_d)_{c2}$ and $(F_d)_{m3}$ (both k_2 and k_3 positive), while the flat bed is found to be stable when F_d is smaller than $(F_d)_{c2}$ and $(F_d)_{m3}$ (both k_2 and k_3 negative).

For $R_d = 40$, the results described above (point i) are found for R_δ approximately smaller than 63, i.e. brick-pattern ripples cannot appear if the flow Reynolds number is smaller than the above value. On the other hand brick-pattern ripples can appear when R_δ exceeds 63 and F_d is larger than $(F_d)_{c2}$, a range of γ being always found within which $\langle b_1\rangle$ and $\langle b_2\rangle$ are both negative. It is worth pointing out that in the range of γ where the theory predicts the possible appearance of brick-pattern ripples, the value of the relative difference between of $(F_d)_{m3}$ from $(F_d)_{c2}$ is always less than 0.1.

On the basis of the present theory and making use of the results described in Blondeaux (1990) and Vittori & Blondeaux (1990), one could attempt to determine the regions of existence of flat-bed, rolling-grain ripples, two-dimensional vortex ripples and brick-pattern ripples in the parameter space. As pointed out previously, because of the strong dependence of the solution of the system (27) on the initial conditions, a precise quantitative definition of the range of validity of the theory is a difficult if not impossible task. Thus in obtaining the results described below, no limit is set on the growth of the different components of bottom perturbation. It follows that, depending on the initial amplitudes of the different components of the bottom perturbation, other nonlinear effects neglected in the present contribution (see for example Vittori & Blondeaux 1990) might turn out to be important and inhibit the growth of one component before the resonant explosion of all the components takes place. In this case brick-pattern ripples would not appear. Thus on the basis of the present theory the parameter space has been divided into a region where brick-pattern ripples might be present and a region where they cannot appear. However, as discussed previously, in the former region other bedforms might also appear depending on the amplitude of the initial perturbations.

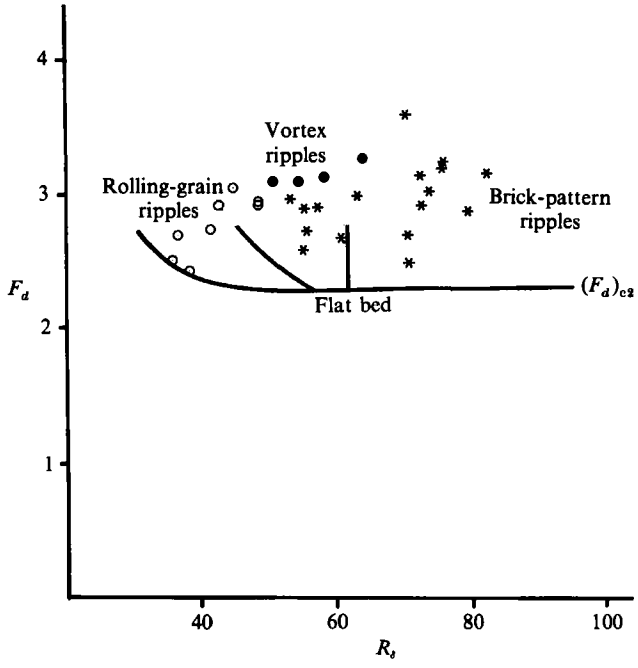

FIGURE 10. Limiting curves dividing the (R_s, F_d)-plane in regions where a flat bed, rolling-grain ripples, two-dimensional vortex ripples, brick-pattern ripples are expected to form ($R_d = 40$, $s = 2.65$, $\mu = 0.15$). Also shown are experimental data by Sleath & Ellis (1978) and Horikawa & Watanabe (1968) for $35 < R_d < 45$ (○, rolling-grain ripples; ●, two-dimensional vortex ripples; *, brick-pattern ripples).

In figure 10 the region of possible existence of brick-pattern ripples is plotted in the $(R_s F_d)$-plane for $R_d = 40$ along with the regions where flat-bed, rolling-grain ripples or two-dimensional vortex ripples are the bedforms predicted by Blondeaux (1990) and Vittori & Blondeaux (1990). Looking at figure 10 it is necessary to recall that the present approach, similarly to that described in Vittori & Blondeaux (1990), is valid only in a neighbourhood of the critical conditions. For this reason the boundary between rolling-grain ripples and two-dimensional vortex ripples and the boundary between two-dimensional vortex ripples and brick-pattern ripples are interrupted after a short distance from the curve dividing the flat-bed region from that of ripples $((F_d - (F_d)_{c2})/(F_d)_{c2}$ less than 0.2).

In order to substantiate the above results, we compare the present theoretical findings with the experimental data available in the literature. Unfortunately the amount of experimental data on brick-pattern ripples is extremely small; indeed to the authors' knowledge the only systematic results available in the literature are those obtained by Sleath & Ellis (1978). In figure 10 the data by Horikawa & Watanabe (1968) on rolling-grain ripples and two-dimensional vortex ripples are also plotted.

It can be seen that all brick-pattern ripples fall within the region predicted by the present theory or close to it. The agreement is also satisfactory considering that the theoretical curves are drawn for R_d equal 40 while the experimental points are characterized by values of R_d falling within the range (35, 45). Moreover it should be noticed that for many experiments F_d is not close to $(F_d)_{c2}$ and only a qualitative agreement should be expected.

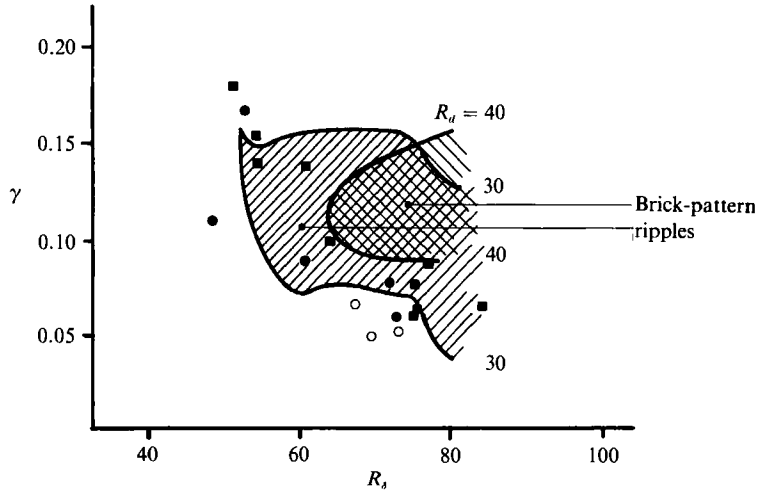

FIGURE 11. Range of γ within which brick-pattern ripples can appear, plotted versus R_δ for $R_d = 30$ and 40 ($s = 2.65$, $\mu = 0.15$). Experimental data by Sleath & Ellis (1978) are for $30 < R_d < 40$. For a description of the symbols see the text.

Another comparison (figure 11) shows the transverse wavenumber measured by Sleath & Ellis (1978) along with the range of γ in which the present theory predicts the possible appearance of brick-pattern ripples. In this case also, the agreement is satisfactory taking into account that the theoretical curves, drawn for $R_d = 30$ and 40, do not depend on the actual value of F_d but require that both $(F_d)-(F_d)_{c2}$ and $(F_d)-(F_d)_{m3}$ be much smaller than 1. On the other hand the experiments are characterized by values of R_d falling within 30 and 40 but the values of F_d are not always close to $(F_d)_{c2}$ and $(F_d)_{m3}$. Experiments where $(F_d-(F_d)_{c2})/(F_d)_{c2} < 0.1$ are denoted by an open circle, those with $0.1 < (F_d-(F_d)_{c2})/(F_d)_{c2} < 0.2$ by a solid circle and those characterized by $(F_d-(F_d)_{c2})/(F_d)_{c2} > 0.2$ by a black square. A comparison between the present theoretical findings and experimental measurements concerning the longitudinal wavenumber β of brick-pattern ripples leads to the conclusion that the present theory underestimates ripple wavelength with a relative error of about 50%. The same quantitative error was found by Blondeaux (1990) in comparing the predicted and measured values of the wavelength of two-dimensional ripples when, as in the case of brick-pattern ripples measured by Sleath & Ellis (1978), the sediment Reynolds number is of the same order as the flow Reynolds number.

For different values of R_d, values of R_δ are found such that three-dimensional perturbations are more unstable than two-dimensional ones. In this case an analysis analogous to that previously described can be used to investigate the possibility of brick-pattern ripple appearance even though some assumptions should be slightly modified.

Indeed it is always possible to assume β equal to α_{c2}, α equal to $\frac{1}{2}\alpha_{c2}$ and a value of F_d which fulfils conditions (22). Alternatively the analysis can be worked out considering α equal to α_{c3} (α_{c3} stands for the longitudinal wavenumber characteristic of the most unstable three-dimensional perturbation) and β equal to $2\alpha_{c3}$. In this case the transverse wavenumber γ should be set equal to γ_c (γ_c stands for the transverse wavenumber characteristic of the most unstable three-dimensional perturbation). Furthermore we must set

$$F_d = (F_d)_{m2} + \epsilon k_2, \quad F_d = (F_d)_{c3} + \epsilon k_3, \tag{30}$$

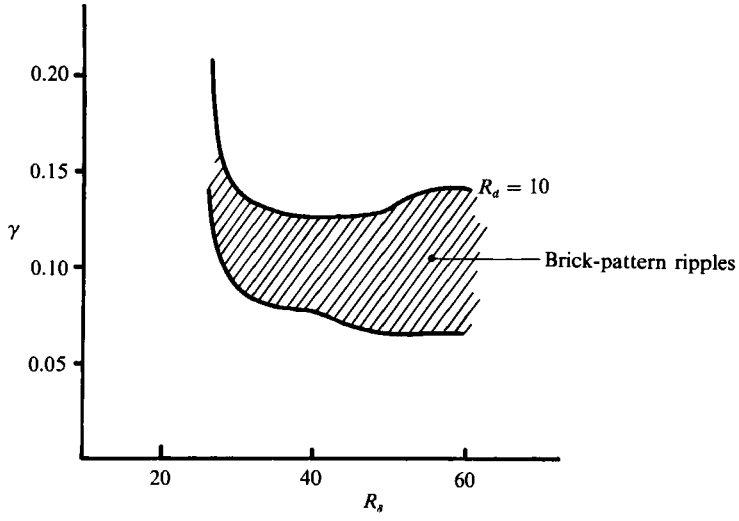

FIGURE 12. Range of γ within which brick-pattern ripples can appear, plotted versus R_δ for $R_d = 10$ ($s = 2.65$, $\mu = 0.15$).

where $(F_d)_{c3}$ is the critical value of the Froude number characteristic of the most unstable three-dimensional perturbation and $(F_d)_{m2}$ is the marginal value of the Froude number characteristic of two-dimensional perturbations with longitudinal wavenumber equal to $2\alpha_{c3}$.

Since it has been assumed, as suggested by the results of the linear stability analysis (§2), that the critical and marginal values of the Froude number do differ by a small amount, it would be also possible to consider different values of the longitudinal and transverse wavenumbers with the only restriction that α should be equal to $\frac{1}{2}\beta$. However, in obtaining quantitative results, only the two limiting cases previously described have been considered and the one that causes the fastest growth of the two-dimensional and three-dimensional components of the bed perturbation has been chosen.

Three-dimensional perturbations are found to be more unstable than two-dimensional ones when, for example, R_d is equal 10. For such a value of the sediment Reynolds number, brick-pattern ripples may appear for flow Reynolds numbers larger than approximately 26. It is worth pointing out that in this situation brick-pattern ripples are always produced by the growth of a two-dimensional waviness which then transfers energy to the three-dimensional waves. It follows that β is equal to α_{c2} and α to $\frac{1}{2}\alpha_{c2}$. In figure 12 the range of γ for which brick-pattern ripples may appear is plotted versus R_δ.

Experimental data by Sleath & Ellis (1978) characterized by R_d falling close to 10 are too few to draw significative comparisons between theoretical findings and experimental data. Moreover it is useful to point out that for such experiments the values of F_d are far from the critical value (namely $(F_d)_{c2}$) for the appearance of ripples. Thus it turns out that in this case the theory can provide only qualitative results. Notwithstanding these limitations it appears that: (i) for the experimental values of the parameters, present theory predicts brick-pattern ripples as a possible bedform, (ii) the experimental transverse wavelengths of brick-pattern ripples fall within the range predicted by the theory (see table 1).

Other experimentalists (Blondeaux, Sleath & Vittori 1988), found for R_d equal to 10, R_δ larger than 26 and F_d larger than $(F_d)_{c2}$ but close to it, other equilibrium bedforms

R_d	R_δ	F_d	Theoretical critical value of F_d for brick-pattern appearance ($R_d = 10$)	Experimental value of γ	Theoretical range of γ ($R_d = 10$)
13.2	46.8	2.61	1.82	0.082	(0.066, 0.126)
18.2	55.0	3.61	1.86	0.088	(0.065, 0.14)

TABLE 1

(namely rolling-grain ripples). At first sight this would appear in contradiction with present theoretical findings. However, in the present theory no limitation is posed on the growth of the amplitudes. As previously said, it might happen that other nonlinear effects inhibit the growth of the amplitudes and prevent the coupling between two-dimensional and three-dimensional bottom perturbations, thus avoiding the appearance of brick-pattern ripples. Indeed for $R_d = 10$ the growth of the three-dimensional components of the bed perturbation is usually driven by the two-dimensional component only when the latter has a very large amplitude, which probably cannot be reached by the two-dimensional waviness close to the marginal conditions, because the effects described in Vittori & Blondeaux (1990) turn out to be important.

Definitive results can then be gained only by means of a fully nonlinear analysis.

4. Discussion

The study of the time development of three-dimensional perturbations of a cohesionless bed subject to an oscillatory flow leads to an explanation of the mechanism of brick-pattern ripple formation: brick-pattern ripples arise because an energy transfer from the two-dimensional components of the bed perturbation to the three-dimensional ones or vice versa leads to the simultaneous growth of all the components and to the appearance of the bottom profile characteristic of brick-pattern ripples.

The present analysis is subject to the same limitations as the analyses described in Blondeaux (1990) and Vittori & Blondeaux (1990). Such limitations derive from the assumptions of a viscous flow over a smooth bottom characterized by the presence of perturbations of small amplitude. It follows that the present analysis holds only for values of R_δ smaller than the critical value for transition to turbulence widely discussed in the literature, when the sediment size d^* is much smaller than the boundary-layer thickness δ^* and when the ripple amplitude is smaller than a critical value for which flow separation occurs (Sleath 1984). As discussed in Vittori & Blondeaux (1990) notwithstanding these limitations, the analyses provide results which can be used to study ripple formation for values of the parameters of physical relevance. Indeed the above assumptions are usually fulfilled underneath gravity waves far from the breaker line when ripples are going to appear.

With respect to the analyses of Blondeaux (1990) and Vittori & Blondeaux (1990), present findings are subject to a further limitation. Indeed, as previously pointed out, for the perturbation approach to be rational the quantities ϵA_i ($i = 1, 2, 3$) should be smaller than 1 (strictly infinitesimal). This limitation simply implies that A_i ($i = 1, 2, 3$) should be smaller than ϵ^{-1}. It follows that when the solution of the system (27) leads to large values of the amplitude functions A_i, the theory is strictly valid within a very small neighbourhood of the marginal stability conditions. As

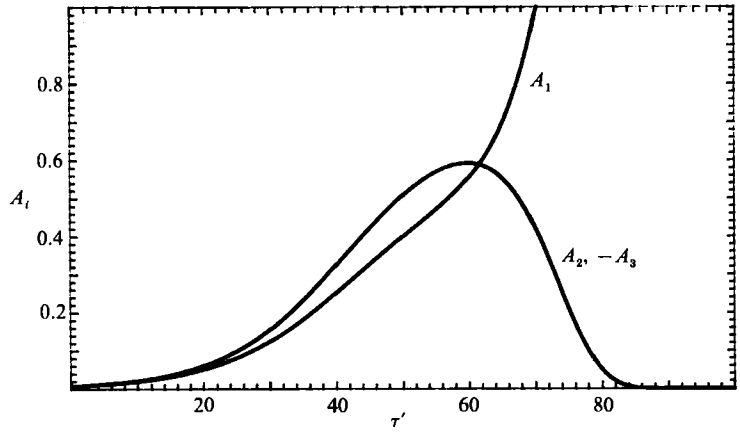

FIGURE 13. Time developments of the amplitudes A_i ($i = 1, 2, 3$) for $\langle a_1 \rangle = \langle b_1 \rangle = 0.1$, $\langle a_2 \rangle = 0.11$, $\langle b_2 \rangle = 0.2$. The initial value of the amplitudes is 0.0075.

discussed in the previous section, because of the strong dependence of the solution of the system (27) on the initial conditions, precise quantitative definition of the validity regions of the theory in the parameter space is a difficult if not impossible task.

The present work however does suggest a mechanism through which three-dimensional perturbations can grow simultaneously with two-dimensional ones, generating three-dimensional ripples and in particular brick-pattern ripples. The accurate prediction of the regions of existence in the parameter space of the different bedforms along with the determination of their characteristics poses a formidable problem which requires knowledge of the fully nonlinear separated flow and related sediment transport.

Finally, it should be mentioned that in presenting the results, only a few values of the parameters have been considered. As previously pointed out, the extent of the parameter space and the length of the calculations have prevented a more complete investigation. It may happen that for different values of R_d, R_δ, F_d other behaviour of the amplitudes A_i ($i = 1, 2, 3$) with respect to those presently discussed can be detected. For example in figure 13 the time development of A_1, A_2 and A_3 is presented for $\langle a_1 \rangle = \langle b_1 \rangle = 0.1$, $\langle a_2 \rangle = 0.11$ and $\langle b_2 \rangle = 0.2$. The initial value of all the amplitudes is 0.0075. It can be seen that for long time only the two-dimensional component grows but there is a time range within which the three-dimensional components grow too. For different values of $\langle a_i \rangle$ and $\langle b_i \rangle$, the temporary growth of A_2 and A_3 could be so strong that an interval may exist within which three-dimensional perturbations have much larger amplitudes than the two-dimensional one. In this case a transitory bedform should appear similar to that sketched in figure 14. It is worthwhile pointing out that the authors, during the experiments described in Blondeaux *et al.* (1988), occasionally observed similar bottom configurations during transition from a stable bottom profile to another one.

Other time developments of A_i ($i = 1, 2, 3$) may be present. A detailed qualitative description of the solutions of the system (27) is given in Weiland & Wilhelmsson (1977) and Craik (1985). However, a long experimental investigation is necessary in order to ascertain which of the possible solutions are true in the field.

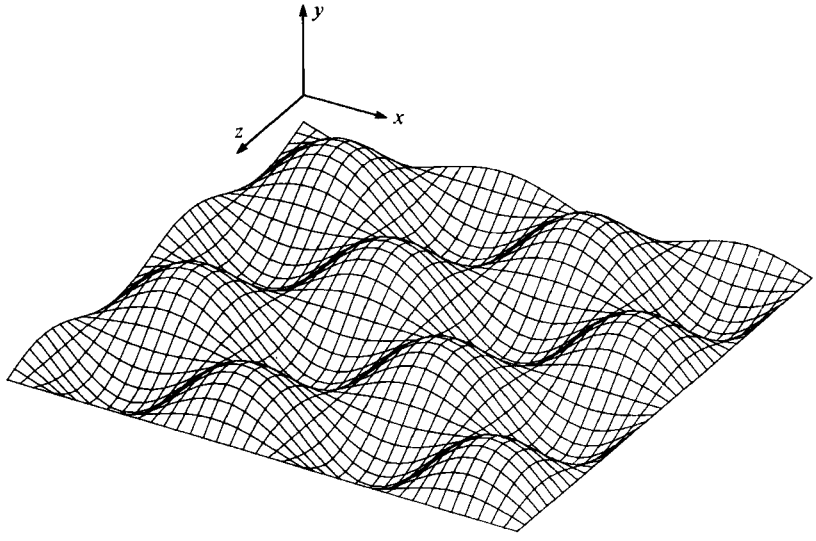

FIGURE 14. Sketch of the bottom configuration predicted by the theory when the three-dimensional components prevail over the two-dimensional ones.

Appendix

The expressions for a_i, b_i and Q_i in (25) are

$$a_1 = 2|2u_0|^{b-1}k_2\frac{\mu R_d}{(F_d)^3_{c2}}b\beta^2,$$

$$b_1 = -2(b-1)\,u_0|2u_0|^{b-3}\left[8\mathrm{i}\alpha b\left(u_{12}\,u_{13}+(u_{13}+u_{12})\frac{\partial u_0}{\partial y}+\left(\frac{\partial u_0}{\partial y}\right)^2\right)\right.$$

$$+4\alpha^2 b\frac{\mu R_d}{(F_d)^2_{c2}}\left(u_{12}+u_{13}+2\frac{\partial u_0}{\partial y}\right)-\left(\frac{\mu R_d}{(F_d)^2_{c2}}\right)^2 2\mathrm{i}(\alpha^3 b-\alpha\gamma^2)$$

$$\left.+8\mathrm{i}\alpha w_{12}\,w_{13}+4\alpha\gamma\frac{\mu R_d}{(F_d)^2_{c2}}(w_{13}-w_{12})\right],$$

$$a_i = 2|2u_0|^{b-1}k_3\frac{\mu R_d}{(F_d)^3_{m3}}(\alpha^2 b+\gamma^2)\quad(i=2,3),$$

$$b_i = -2(b-1)\,u_0|2u_0|^{b-3}\left[4\mathrm{i}b(\beta-\alpha)\left(u_{11}\,\bar{u}_{1(5-i)}+(\bar{u}_{1(5-i)}u_{11})\frac{\partial u_0}{\partial y}+\left(\frac{\partial u_0}{\partial y}\right)^2\right)\right.$$

$$+2\gamma^2\frac{\mu R_d}{(F_d)^2_{m3}}\left(u_{11}+\frac{\partial u_0}{\partial y}+\frac{\beta}{\gamma}\bar{w}_{1(5-i)}\right)$$

$$+2b(\beta-\alpha)\frac{\mu R_d}{(F_d)^2_{m3}}$$

$$\times\left(\beta\bar{u}_{1(5-i)}-\alpha u_{11}+(\beta-\alpha)\frac{\partial u_0}{\partial y}\right)+\left(\frac{\mu R_d}{(F_d)^2_{m3}}\right)^2\mathrm{i}\beta(b\alpha(\beta-\alpha)-\gamma^2)$$

$$\left.+(-1)^i 4\mathrm{i}\gamma\bar{w}_{1(5-i)}\left(u_{11}+\frac{\partial u_0}{\partial y}\right)\right]\quad(i=2,3),$$

$$Q_1 = |2u_0|^{b-1} b\left[2i\beta\left(u'_{21}+\frac{\partial u_0}{\partial y}\right)+\frac{\mu R_d}{(F_d)^2_{c2}}\beta^2\right],$$

$$Q_i = |2u_0|^{b-1}\left[2i\alpha b\left(u'_{2i}+\frac{\partial u_0}{\partial y}\right)+(-1)^i 2i\gamma w'_{2i}+\frac{\mu R_d}{(Fd)^2_{m3}}(\alpha^2 b+\gamma^2)\right] \quad (i=2,3).$$

In all the above expressions the functions of y are evaluated at $y = R_d/2R_\delta$.

REFERENCES

ALLEN, J. R. L. 1984 *Developments in Sedimentology*. Elsevier.

BAGNOLD, R. A. 1946 Motion of waves in shallow water. Interaction of waves and sand bottoms. *Proc. R. Soc. Lond.* A **187**, 1–15.

BLONDEAUX, P. 1990 Sand ripples under sea waves. Part 1. Ripple formation. *J. Fluid Mech.* **218**, 1–17.

BLONDEAUX, P. & SEMINARA, G. 1985 A unified bar–bend theory of river meanders. *J. Fluid Mech.* **157**, 449–470.

BLONDEAUX, P., SLEATH, J. F. A. & VITTORI, G. 1988 Experimental data on sand ripples in an oscillatory flow. *Rep.* 01/88. Hydraulic Institute, University of Genoa.

COLOMBINI, M., SEMINARA, G. & TUBINO, M. 1987 Finite-amplitude alternate bars. *J. Fluid Mech.* **181**, 213–232.

CRAIK, A. D. D. 1971 Non-linear resonant instability in boundary layers. *J. Fluid Mech.* **50**, 393–413.

CRAIK, A. D. D. 1985 *Wave Interactions and Fluid Flows*. Cambridge University Press.

FREDSØE, J. 1974 On the developments of dunes on erodible channels. *J. Fluid Mech.* **64**, 1–16.

GRASS, J. A. & AYOUB, N. M. 1982 Bed load transport of fine sand by laminar and turbulent flow. In *Proc. 18th Coastal Eng. Conf.* (ed. B. L. Edge) pp. 1589–1599.

HARA, T. & MEI, C. C. 1990 Centrifugal instability of an oscillatory flow over periodic ripples. *J. Fluid Mech.* **217**, 1–32.

HORIKAWA, K. & WATANABE, A. 1968 Laboratory study on oscillatory boundary layer flow. *Coastal Eng. Japan* **11**, 13–28.

PARKER, G. 1976 On the cause and characteristic scales of meandering and braiding in rivers. *J. Fluid Mech.* **76**, 457–480.

RICHARDS, K. J. 1980 The formation of ripples and dunes on an erodible bed. *J. Fluid Mech.* **99**, 597–618.

SEMINARA, G. & HALL, P. 1976 The centrifugal instability of a Stokes layer theory. *Proc. R. Soc. Lond.* A **350**, 299–316.

SLEATH, J. F. A. 1984 *Sea Bed Mechanics*. Wiley.

SLEATH, J. F. A. & ELLIS, A. C. 1978 Ripple geometry in oscillatory flow. *CUED/A – Hydraulics*/TR 2, University of Cambridge, Engineering Department.

SMITH, F. T. & STEWART, P. A. 1987 The resonant-triad nonlinear interaction in boundary-layer transition. *J. Fluid Mech.* **179**, 227–252.

STOKES, A. G. 1851 On the effect of the internal friction of fluids on the motion of pendulums. *Trans. Camb. Phil. Soc.* **9**, 20–21.

SUMER, M. & BAKIOGLU, M. 1984 On the formation of ripples on an erodible bed. *J. Fluid Mech.* **144**, 177–190.

VITTORI, G. 1992 Flow field induced by sea waves over brick-pattern ripples. *J. Hydraul. Engng ASCE* (to appear).

VITTORI, G. & BLONDEAUX, P. 1990 Sand ripples under sea waves. Part 2. Finite amplitude development. *J. Fluid Mech.* **218**, 19–39.

WEILAND, J. & WILHELMSSON, H. 1977 *Coherent Nonlinear Interaction of Waves in Plasmas*. Pergamon.